

Cite this: *J. Mater. Chem. C*, 2020, **8**, 7454Received 10th February 2020,
Accepted 12th April 2020

DOI: 10.1039/d0tc00683a

rsc.li/materials-c

Effects of alkyl chain length and anion on the optical and electrochemical properties of AIE-active α -cyanostilbene-containing triphenylamine derivatives†

Sin-Yu Chen,^a Min-Hao Pai^a and Guey-Sheng Liou^{id} *^{ab}

A series of aggregation induced emission (AIE)-active and redox-active α -cyanostilbene-containing triphenylamine derivatives with different alkyl chain lengths and anions were successfully synthesized, and their optical, photoluminescent and electrochromic behaviors were investigated. In addition, the intrinsically ambipolar system was generated by incorporating the pyridinium moiety, which serves as a charge storage unit to effectively balance the charge during the electrochemical oxidation redox process. The photoluminescent performance of the resulting AIE- and redox-active materials in solution, aggregated and solid states was influenced by the different alkyl chains as well as anions.

Introduction

Pyridinium salts have attracted a lot of attention because of the common skeleton that has been found in various kinds of natural and bioactive structures in the last few decades.¹ Based on the organic chemistry, the pyridinium salts have been utilized as key intermediates for applications in drug delivery, as sensors for detecting heavy metal ions in sewage, as chemotherapeutics, and so on.² In 2019, B. Z. Tang's group utilized the cyanostilbene unit as D- π -A-based AIEgens to enhance the TITC effect, resulting in red-shifted emission to obtain better bioimaging, and incorporated the pyridine moiety into the cyanostilbene derivatives to increase their biocompatibility in the membranes and mitochondria of live cells.³ In addition, the pyridinium moiety resembles the structure of viologens, which are widely applied as cathodic electrochromic (EC) material, and could thus endow molecular structures with electron-withdrawing capability, leading to red-shifted absorption and photoluminescent (PL) behaviors.⁴

Aggregation-induced emission (AIE) was first coined in 2001 by Tang's group.⁵ This phenomenon, in contrast to the traditional aggregation-caused quenching (ACQ), features strong emission in the aggregated and solid states on account of the restriction of intramolecular motions. By incorporating an AIE-active unit,

the PL characteristic of ACQ could be changed to the AIE behavior; this should be a facile approach to successfully acquire highly fluorescent materials in solid state and could broaden the applications in optoelectronic technology.⁶

In this article, a series of α -cyanostilbene-containing redox-active triphenylamine (TPA) derivatives with pyridinium salts (**TPA-Py-*n*-Br**, **TPA-Py-*n*-BF₄**, **diOMe-TPA-Py-*n*-Br**, **diOMe-TPA-Py-*n*-BF₄**) were designed and synthesized to endow the targeted materials with AIE-active PL characteristic. Meanwhile, ambipolar structure could also be obtained by introducing the TPA moiety as electron donor and the pyridinium unit as electron acceptor that could play a role in trapping charges during the electrochemical oxidation redox process.⁷ Furthermore, the effects of alkyl chain length and anions on the optical, PL and electrochemical behaviors of these resulting materials are discussed extensively in this work.

Experimental section

Materials

Commercially available diphenylamine (Alfa), 4-bromobenzaldehyde (AK Scientific), phenylacetonitrile (ACROS), 4-bromophenylacetonitrile (Alfa), *p*-anisidine (ACROS), 4-bromoanisole (Alfa), tetrakis(triphenylphosphine)palladium (0) (AK Scientific), 4-pyridylboronic acid (Matrix), bromoethane (Alfa), 1-bromoheptane (Alfa), tetrabutylammonium bromide (TBAB) (Alfa) and other reagents were used as received. TBAB was ion exchanged with sodium tetrafluoroborate (NaBF₄) to obtain tetrabutylammonium tetrafluoroborate (TBABF₄), which served as the electrolyte during electrochromic measurement. The ion exchange procedure was to mix both saturated aqueous solutions of TBAB and NaBF₄ and recrystallize the white powder from ethyl acetate.

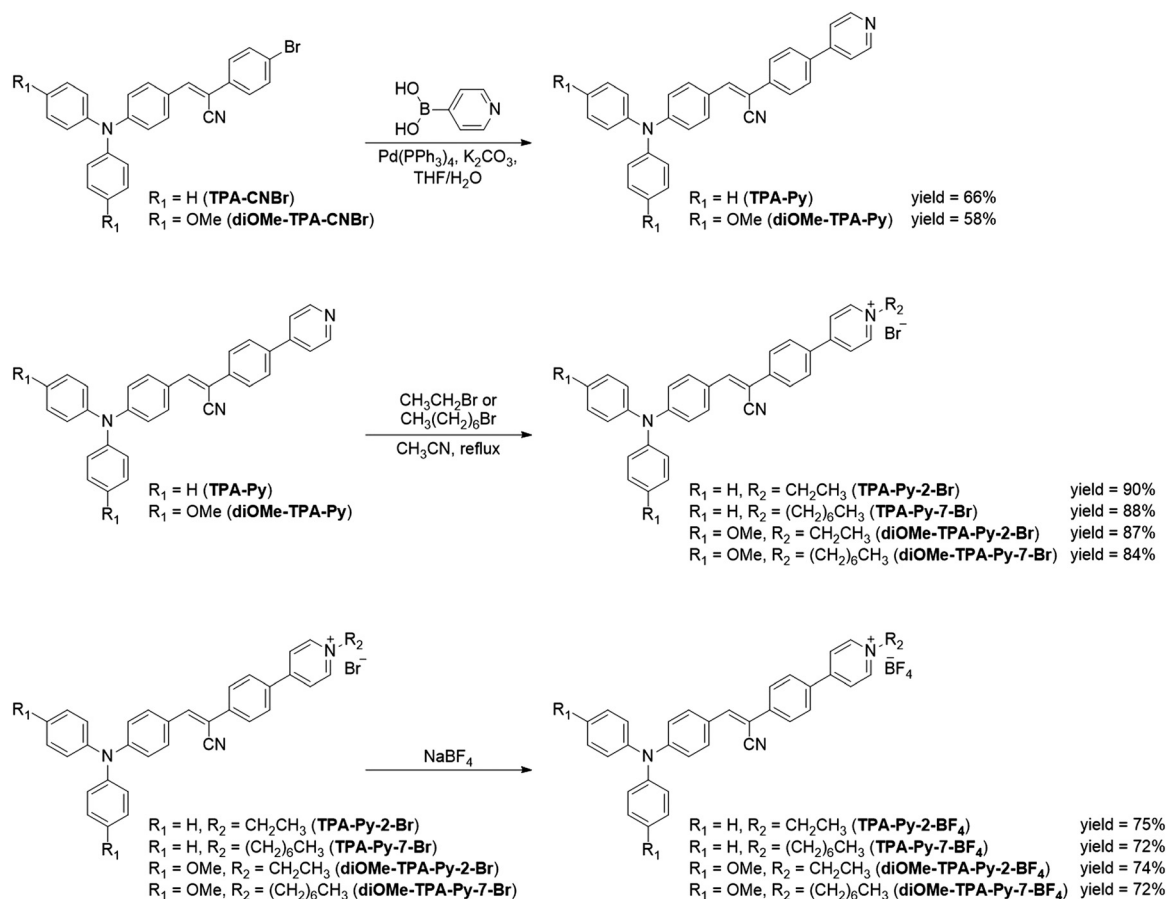
^a Institute of Polymer Science and Engineering, National Taiwan University, No. 1, Sec. 4, Roosevelt Rd., Taipei, 10617, Taiwan. E-mail: gshliou@ntu.edu.tw

^b Advanced Research Center for Green Materials Science and Technology, National Taiwan University, Taipei 10617, Taiwan

† Electronic supplementary information (ESI) available. CCDC 1983090–1983094. For ESI and crystallographic data in CIF or other electronic format see DOI: 10.1039/d0tc00683a

Monomer synthesis

TPA-Py⁸ and diOMe-TPA-Py were synthesized by the Suzuki reaction of TPA-CNBr and diOMe-TPA-CNBr with 4-pyridylboronic acid in a yield of 66% and 58%, respectively.⁹ Next, alkylation process was used to prepare TPA-Py-*n*-Br and diOMe-TPA-Py-*n*-Br, and *n* was determined as 2 and 7 when bromoethane and 1-bromoheptane were utilized, respectively. The reaction routes and yields of TPA-Py-*n*-Br and diOMe-TPA-Py-*n*-Br are illustrated in Scheme 1. The subsequent ion exchange reaction proceeded just by mixing the solution of NaBF₄/solvent (water or methanol) and TPA-Py-*n*-Br/acetone (or diOMe-TPA-Py-*n*-Br/DCM). FT-IR and NMR were used to identify the new structures of these two series of compounds. NMR spectra demonstrated good agreement of the proposed molecular structures, shown in Fig. S1–S24 (ESI[†]). However, the characteristic peak of structures before and after anion exchange could not be identified lucidly in the NMR spectra (Fig. S17–S24, ESI[†]). Therefore, the FT-IR spectra (Fig. S25, ESI[†]) were utilized to check whether the characteristic peak of BF₄⁻ anion (1100–1000 cm⁻¹) appeared, and the results were in agreement with the proposed molecular structures of TPA-Py series and diOMe-TPA-Py series. TPA-Py-*n*-Br: m.p. (TPA-Py-2-Br) 120–122 °C; m.p. (TPA-Py-7-Br) 184–186 °C. ¹H NMR (400 MHz, DMSO-*d*₆, δ) of TPA-Py-2-Br: 9.16 (d, 2H), 8.59 (d, 2H), 8.23 (d, 2H), 8.14 (s, 1H), 7.97 (d, 2H), 7.92 (d, 2H), 7.40 (t, 4H), 7.21–7.15 (m, 6H), 6.95 (d, 2H), 4.60 (t, 2H), 1.94 (m, 2H), 1.28 (m, 8H), 0.86 (t, 3H). ¹³C-NMR (100 MHz, DMSO-*d*₆, δ) of TPA-Py-2-Br: 153.4 (C¹⁶), 150.0 (C⁵), 145.8 (C⁴), 144.6 (C¹⁸), 143.9 (C⁹), 137.8 (C¹²), 133.1 (C¹⁵), 131.3 (C⁷), 129.9 (C²), 128.9 (C¹⁴), 126.3 (C¹³), 125.8 (C³), 125.6 (C⁸), 125.0 (C¹), 124.3 (C¹⁷), 119.5 (C⁶), 118.2 (C¹¹), 104.6 (C¹⁰), 55.48 (C¹⁹), 16.32 (C²⁰). ¹³C-NMR (100 MHz, DMSO-*d*₆, δ) of TPA-Py-7-Br: 153.4 (C¹⁶), 150.0 (C⁵), 145.8 (C⁴), 144.8 (C¹⁸), 143.9 (C⁹), 137.8 (C¹²), 133.0 (C¹⁵), 131.3 (C⁷), 129.9 (C²), 128.9 (C¹⁴), 126.3 (C¹³), 125.8 (C³), 125.7 (C⁸), 125.0 (C¹), 124.3 (C¹⁷), 119.5 (C⁶), 118.2 (C¹¹), 104.6 (C¹⁰), 59.86 (C¹⁹), 31.02–21.96 (C²⁴–C²⁰), 13.90 (C²⁵). TPA-Py-*n*-BF₄: m.p. (TPA-Py-2-BF₄) 231–235 °C; m.p. (TPA-Py-7-BF₄) 228–229 °C. ¹H NMR (400 MHz, DMSO-*d*₆, δ) of TPA-Py-2-BF₄: 9.13 (d, 2H), 8.58 (d, 2H), 8.22 (d, 2H), 8.14 (s, 1H), 7.98 (d, 2H), 7.92 (d, 2H), 7.42 (t, 4H), 7.23–7.17 (m, 6H), 6.97 (d, 2H), 4.62 (m, 2H), 1.58 (t, 3H). ¹H NMR (400 MHz, DMSO-*d*₆, δ) of TPA-Py-7-BF₄: 9.11 (d, 2H), 8.57 (d, 2H), 8.22 (d, 2H), 8.14 (s, 1H), 7.98 (d, 2H), 7.92 (d, 2H), 7.41 (t, 4H), 7.23–7.18 (m, 6H), 6.97 (d, 2H), 4.57 (t, 2H), 1.94 (m, 2H), 1.29 (m, 8H), 0.86 (t, 3H). ¹³C-NMR (100 MHz, DMSO-*d*₆, δ) of TPA-Py-2-BF₄: 153.3 (C¹⁶), 149.9 (C⁵), 145.7 (C⁴), 144.4 (C¹⁸), 143.7 (C⁹), 137.6 (C¹²), 132.9 (C¹⁵), 131.1 (C⁷), 129.8 (C²), 128.7 (C¹⁴),



Scheme 1 Synthetic routes of TPA-Py-*n*-Br, TPA-Py-*n*-BF₄, diOMe-TPA-Py-*n*-Br and diOMe-TPA-Py-*n*-BF₄.

126.1 (C¹³), 125.7 (C³), 125.5 (C⁸), 124.8 (C¹), 124.2 (C¹⁷), 119.4 (C⁶), 118.1 (C¹¹), 104.5 (C¹⁰), 55.40 (C¹⁹), 16.13 (C²⁰). ¹³C-NMR (100 MHz, DMSO-*d*₆, δ) of **TPA-Py-7-BF₄**: 153.5 (C¹⁶), 150.0 (C⁵), 145.8 (C⁴), 144.7 (C¹⁸), 143.9 (C⁹), 137.8 (C¹²), 133.1 (C¹⁵), 131.3 (C⁷), 129.9 (C²), 128.9 (C¹⁴), 126.3 (C¹³), 125.8 (C³), 125.6 (C⁸), 125.0 (C¹), 124.3 (C¹⁷), 119.5 (C⁶), 118.2 (C¹¹), 104.6 (C¹⁰), 59.95 (C¹⁹), 31.01–21.96 (C²⁴–C²⁰), 13.89 (C²⁵). **diOMe-TPA-Py-*n*-Br**: m.p. (**diOMe-TPA-Py-2-Br**) 207–211 °C; m.p. (**diOMe-TPA-Py-7-Br**) 225–227 °C. ¹H NMR (400 MHz, DMSO-*d*₆, δ) of **diOMe-TPA-Py-2-Br**: 9.16 (d, 2H), 8.56 (d, 2H), 8.18 (d, 2H), 8.04 (s, 1H), 7.89 (d, 2H), 7.83 (d, 2H), 7.13 (t, 4H), 6.96 (m, 4H), 6.71 (d, 2H), 4.65 (m, 2H), 3.74 (s, 6H), 1.55 (t, 3H). ¹H NMR (400 MHz, DMSO-*d*₆, δ) of **diOMe-TPA-Py-7-Br**: 9.20 (d, 2H), 8.60 (d, 2H), 8.21 (d, 2H), 8.09 (s, 1H), 7.92 (d, 2H), 7.86 (d, 2H), 7.15 (m, 4H), 6.98 (m, 4H), 6.73 (d, 2H), 4.63 (t, 2H), 3.76 (s, 6H), 1.94 (m, 2H), 1.28 (m, 8H), 0.85 (t, 3H). ¹³C-NMR (100 MHz, DMSO-*d*₆, δ) of **diOMe-TPA-Py-2-Br**: 156.9 (C²), 153.4 (C¹⁷), 151.1 (C⁶), 144.6 (C¹⁹), 144.0 (C¹⁰), 138.3 (C⁵), 138.0 (C¹⁶), 132.7 (C¹³), 131.4 (C⁸), 128.8 (C¹⁵), 128.0 (C⁴), 126.1 (C¹⁴), 124.2 (C¹⁸), 123.7 (C⁹), 118.5 (C¹²), 116.4 (C⁷), 115.2 (C³), 103.1 (C¹¹), 55.45 (C²⁰), 55.35 (C¹), 16.35 (C²¹). ¹³C-NMR (100 MHz, DMSO-*d*₆, δ) of **diOMe-TPA-Py-7-Br**: 157.3 (C²), 153.7 (C¹⁷), 151.4 (C⁶), 145.1 (C¹⁹), 144.3 (C¹⁰), 138.7 (C⁵), 138.4 (C¹⁶), 133.0 (C¹³), 131.7 (C⁸), 129.2 (C¹⁵), 128.3 (C⁴), 126.4 (C¹⁴), 124.5 (C¹⁸), 124.1 (C⁹), 118.8 (C¹²), 116.7 (C⁷), 115.6 (C³), 103.4 (C¹¹), 60.12 (C²⁰), 55.70 (C¹), 31.41–22.35 (C²¹–C²⁵), 14.27 (C²⁶). **diOMe-TPA-Py-*n*-BF₄**: m.p. (**diOMe-TPA-Py-2-BF₄**): 183–188 °C; m.p. (**diOMe-TPA-Py-7-BF₄**) 148–151 °C. ¹H NMR (400 MHz, DMSO-*d*₆, δ) of **diOMe-TPA-Py-2-BF₄**: 9.11 (d, 2H), 8.57 (d, 2H), 8.22 (d, 2H), 8.07 (s, 1H), 7.94 (d, 2H), 7.86 (d, 2H), 7.18 (t, 4H), 7.00 (m, 4H), 6.76 (d, 2H), 4.62 (m, 2H), 3.76 (s, 6H), 1.57 (t, 3H). ¹H NMR (400 MHz, DMSO-*d*₆, δ) of **diOMe-TPA-Py-7-BF₄**: 9.10 (d, 2H), 8.56 (d, 2H), 8.20 (d, 2H), 8.08 (s, 1H), 7.95 (d, 2H), 7.86 (d, 2H), 7.18 (m, 4H), 6.99 (m, 4H), 6.75 (d, 2H), 4.57 (t, 2H), 3.77 (s, 6H), 1.94 (m, 2H), 1.29 (m, 8H), 0.86 (t, 3H). ¹³C-NMR (100 MHz, DMSO-*d*₆, δ) of **diOMe-TPA-Py-2-BF₄**: 157.0 (C²), 153.5 (C¹⁷), 151.1 (C⁶), 144.5 (C¹⁹), 144.0 (C¹⁰), 138.4 (C⁵), 138.1 (C¹⁶), 132.8 (C¹³), 131.4 (C⁸), 128.8 (C¹⁵), 128.1 (C⁴), 126.1 (C¹⁴), 124.2 (C¹⁸), 123.7 (C⁹), 118.5 (C¹²), 116.4 (C⁷), 115.3 (C³), 103.1 (C¹¹), 55.55 (C²⁰), 55.33 (C¹), 16.28 (C²¹). ¹³C-NMR (100 MHz, DMSO-*d*₆, δ) of **diOMe-TPA-Py-7-BF₄**: 157.3 (C²), 153.8 (C¹⁷), 151.5 (C⁶), 145.1 (C¹⁹), 144.4 (C¹⁰), 138.7 (C⁵), 138.5 (C¹⁶), 133.1 (C¹³), 131.7 (C⁸), 129.2 (C¹⁵), 128.4 (C⁴), 126.4 (C¹⁴), 124.6 (C¹⁸), 124.1 (C⁹), 118.9 (C¹²), 116.7 (C⁷), 115.6 (C³), 103.5 (C¹¹), 60.31 (C²⁰), 55.68 (C¹), 31.39–22.34 (C²¹–C²⁵), 14.27 (C²⁶).

Measurements

The OptiMelt automated melting point system and differential scanning calorimetry (DSC) were used to detect the melting point of the compounds at the scan rate of 10 °C min⁻¹. ¹H and ¹³C NMR spectra were conducted on a Bruker DPX-400 MHz FT-NMR using chloroform-*d* (CDCl₃) and dimethyl sulfoxide (DMSO-*d*₆) as solvents, and tetramethylsilane (TMS; δ = 0 ppm) was chosen as internal reference. In addition, peak multiplicity was marked as follows: s, singlet; d, doublet; t, triplet; m, multiplet. Fourier transform infrared (FT-IR) spectra were recorded using a PerkinElmer Spectrum 100 model FT-IR spectrometer by

incorporating samples in potassium bromide (KBr) disks. Cyclic voltammetry (CV) was measured with the optically transparent thin-layer electrochemical (OTTLE) cell and Ag/AgCl; KCl (sat.) served as the reference electrode. Spectroelectrochemistry was implemented in a 1 cm quartz cell by means of Hewlett-Packard 8453 UV-vis diode array spectrophotometer. ITO-coated glass was utilized as the working electrode, a platinum wire served as the counter electrode, and an Ag/AgCl cell was used as the reference electrode. PL quantum yield (Φ_F) of materials in different solvents was measured by using quinine sulfate dissolved in 1 N sulfuric acid as a reference standard (Φ_F = 0.546), and the Φ_F of small molecules in solid state was measured by a calibrated integrating sphere.

Results and discussion

Monomer synthesis and characterization

The new targeted materials, **TPA-Py-*n*-Br**, **TPA-Py-*n*-BF₄**, **diOMe-TPA-Py-*n*-Br** and **diOMe-TPA-Py-*n*-BF₄**, were successfully prepared *via* the procedures depicted in Scheme 1. The intermediate compounds of **TPA-CNBr** and **diOMe-TPA-CNBr** were synthesized according to the previous literature;^{9c,10} **TPA-Py** and **diOMe-TPA-Py** were obtained by the Suzuki reaction of **TPA-CNBr** and **diOMe-TPA-CNBr** with 4-pyridylboronic acid in a yield of 66% and 58%, respectively. Afterwards, alkylation reaction was used to produce **TPA-Py-*n*-Br** and **diOMe-TPA-Py-*n*-Br**, and *n* was determined as 2 and 7 when bromoethane and 1-bromoheptane were utilized, respectively. The further step of ion exchange reaction proceeded just by mixing NaBF₄/solvent (water or methanol) solution and **TPA-Py-*n*-Br**/acetone (or **diOMe-TPA-Py-*n*-Br**/dichloromethane). FT-IR and NMR analysis were used to identify the structures of these new compounds. NMR spectra summarized in Fig. S1–S24 (ESI[†]) demonstrate good agreement of the proposed molecular structures. However, the characteristic peaks of structures before and after anion exchange could not be identified clearly from the NMR spectra.¹¹ Therefore, the FT-IR spectra (Fig. S25, ESI[†]) were utilized to confirm and distinguish the characteristic peak of BF₄⁻ anion (1100–1000 cm⁻¹) with bromide anion according to the previous literature,¹² and the results are also in good agreement with the proposed molecular structures for both the **TPA-Py** and **diOMe-TPA-Py** series.

Optical properties

The optical properties of these cyanostilbene-containing TPA derivatives were investigated by UV-vis spectrophotometry and photoluminescence (PL) spectroscopy. The UV-Vis absorption and PL emission spectra of the obtained materials, both in dimethyl sulfoxide (DMSO) solution and solid state, are depicted in Fig. 1 and 2, respectively. In contrast to the structures containing an ethyl chain, the materials with heptyl chain exhibited bathochromic effect on the maximum absorption peaks (λ_{abs}) in DMSO solution (**TPA-Py-2-Br/BF₄**: 449 nm, **TPA-Py-7-Br/BF₄**: 451 nm) and solid state (**TPA-Py-2-Br/BF₄**: 470 nm, **TPA-Py-7-Br/BF₄**: 475 nm). Nevertheless, the anion effect on the maximum absorption peaks (λ_{abs}) both in DMSO solution and solid state could not be observed. The same phenomenon was obtained in the series of

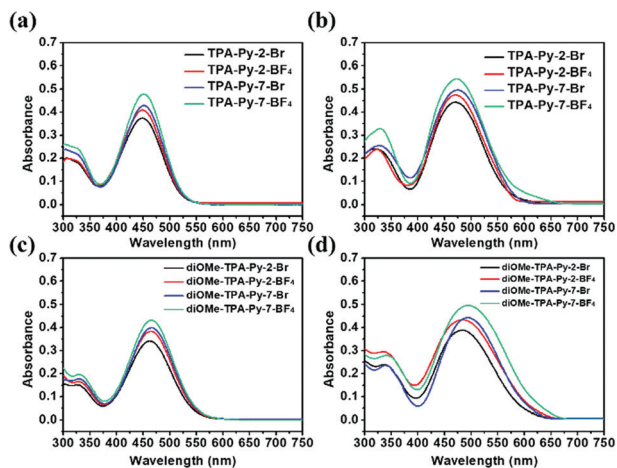


Fig. 1 Absorption spectra of TPA-Py series in (a) DMSO solution (10 μM) and (b) solid state; diOMe-TPA-Py series in (c) DMSO solution (10 μM) and (d) solid state.

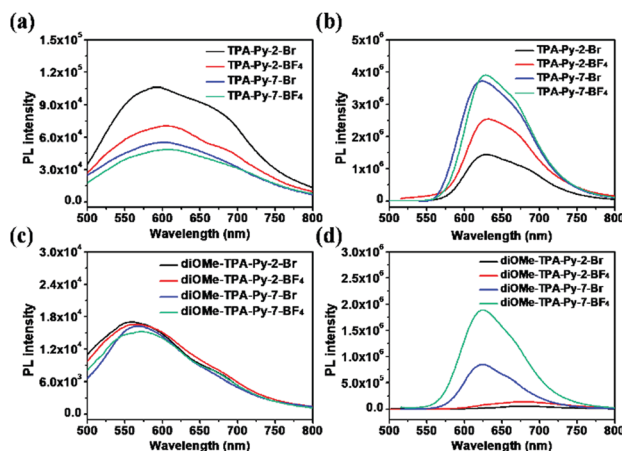


Fig. 2 PL spectra of TPA-Py series in (a) DMSO solution (10 μM) and (b) solid state; diOMe-TPA-Py series in (c) DMSO solution (10 μM) and (d) solid state.

diOMe-TPA-Py (diOMe-TPA-Py-2-Br/BF₄ in solution: 463 nm, diOMe-TPA-Py-7-Br/BF₄ in solution: 466 nm; diOMe-TPA-Py-2-Br/BF₄ in solid: 484 nm, diOMe-TPA-Py-7-Br/BF₄ in solid: 494 nm). As mentioned above, by introducing the auxochrome of dimethoxy groups into the diOMe-TPA-Py series, the absorption wavelength (λ_{abs}) of the corresponding compounds revealed red-shifted characteristics both in DMSO solution and solid state due to the stronger donor-acceptor ability, as summarized in Table 1. The PL emission peaks (λ_{em}) of these materials in DMSO solution showed a bathochromic shift as the bromide anion (Br⁻) was replaced by the tetrafluoroborate anion (BF₄⁻) (TPA-Py-2-Br: 592 nm, TPA-Py-2-BF₄: 605 nm) as well as with the increasing chain length of alkyl groups (TPA-Py-2-Br: 592 nm, TPA-Py-7-Br: 603 nm). In addition, the λ_{em} in solid state also red-shifted as Br⁻ was exchanged to BF₄⁻ (TPA-Py-2-Br: 629 nm, TPA-Py-2-BF₄: 632 nm), while it revealed a blue shift in the case of molecular structures with the longer alkyl chain (TPA-Py-2-Br: 629 nm, TPA-Py-7-Br: 624 nm), which should be ascribed to the suppressed


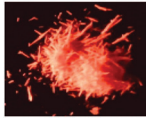

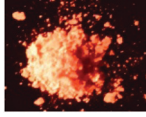



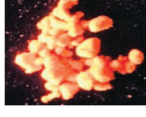



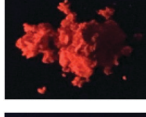



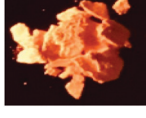
interchain interaction of the aromatic units within the crystalline lattice of the materials, bringing about an apparently hypsochromic emission shift in the solid state.¹³ In the aspect of PL intensity, the alkyl chain interferes with π - π stacking, leading to higher quantum yield in solid state.¹⁴ Moreover, there is a special effect called heavy atom effect for the bromide anion, which would influence the fluorescence behavior, resulting in PL quenching caused by the probability of intersystem crossing. Intersystem crossing is a non-radiative transition between two isoenergetic vibrational levels belonging to electronic states of different spin multiplicities, and may be fast enough (10^{-7} – 10^{-9} s) to compete with other pathways of de-excitation from S₁ state (the fluorescence and internal conversion S₁ \rightarrow S₀), which could explain why molecular structures with BF₄⁻ (TPA-Py-*n*-BF₄ and diOMe-TPA-Py-*n*-BF₄) have stronger fluorescence intensity and higher quantum yield in solid state.

Photoluminescent properties

Aggregation-induced emission (AIE) effect. All these cyano-stilbene-containing TPA compounds exhibited high solubility in common organic solvents like DMSO, but were insoluble in water. The AIE characteristics could be confirmed in various water/DMSO fractions ($f_w = 0$ –99%) at a concentration of 10 μM , and the photos demonstrating PL behaviors and relative emission intensity (I/I_0) taken under UV irradiation are summarized in Fig. 3 (TPA-Py-7-Br), Fig. 4 (TPA-Py-7-BF₄) and Fig. S26–S31 (ESI[†]). The formation of aggregates from molecules appeared as water content increased within the water/DMSO mixture, and the intramolecular motions could be restricted by virtue of the aggregation, resulting in stronger emission intensity.

All the compounds of TPA-Py series displayed AIE features in solution and aggregated states, as illustrated in Fig. 3, 4, and Fig. S26 and S27 (ESI[†]). The photos of emissive behaviors for TPA-Py-7-Br at different fractions of water/DMSO mixture are shown in Fig. 3a. The AIE characteristic of TPA-Py-7-Br depicted in Fig. 3b reveals the emission peak of TPA-Py-7-Br at 603 nm, with only 0.08% quantum yield (Φ_F) in pure DMSO solution, estimated by quinine sulfate as standard ($\Phi_F = 0.546$ dissolved in 1 N H₂SO₄ in 10 μM concentration), indicating the weak emitting ability in solution state. When the fraction of poor solvent (water) gradually increased in the solution, the PL intensity of TPA-Py-7-Br was enhanced rapidly at the water fraction, f_w , of 80%, caused by the AIE effect. Fig. 3c can be used to demonstrate the quantification of AIE of TPA-Py-7-Br; the emission intensity in the aggregated state could reach around 13-fold that in pure DMSO solution. A similar PL behavior to TPA-Py-7-Br could be observed for TPA-Py-7-BF₄ (the maximum fluorescence intensity at 608 nm in pure DMSO solution with 0.07% quantum yield), as depicted in Fig. 4, while the relative PL intensity of the aggregated state (I/I_0) could reach about 49-fold, which is much higher than that in pure DMSO solution. Consequently, TPA-Py-7-BF₄ revealed higher value of α_{AIE} (TPA-Py-7-Br: 234, TPA-Py-7-BF₄: 272) and quantum yield in solid state than TPA-Py-7-Br (TPA-Py-7-Br: 17.6%, TPA-Py-7-BF₄: 18.7%). A similar trend related to the quantum yield in solid state could also be observed between TPA-Py-2-Br and TPA-Py-2-BF₄ (TPA-Py-2-Br: 9.1%, TPA-Py-2-BF₄: 13.1%), and the α_{AIE} values of

Table 1 Photoluminescent properties of TPA-Py series and diOMe-TPA-Py series

	λ_{abs}^a (solution)	λ_{em}^a (solution)	λ_{abs}^a (solid)	λ_{em}^a (solid)	Φ_{F}^b (%) (solution)	Φ_{F}^c (%) (solid)	α_{AIE}^d	Under room light	Under UV light (365 nm)
TPA-Py-2-Br	449	592	470	629	0.14	9.1	63		
TPA-Py-2-BF ₄	449	605	470	632	0.09	13.1	149		
TPA-Py-7-Br	451	603	475	624	0.08	17.6	234		
TPA-Py-7-BF ₄	451	608	475	629	0.07	18.7	272		
diOMe-TPA-Py-2-Br	463	560	484	677	0.02	0.26	13		
diOMe-TPA-Py-2-BF ₄	463	564	484	678	0.02	1.51	76		
diOMe-TPA-Py-7-Br	466	567	494	624	0.02	4.27	214		
diOMe-TPA-Py-7-BF ₄	466	570	494	625	0.02	9.88	494		

^a Observed from absorption and emission spectra in dilute DMSO solutions (10^{-5} M). ^b Fluorescence quantum yield determined using quinine sulfate ($\Phi_{\text{F}} = 54.6\%$ in 0.1 N sulfuric acid) as standard. ^c Fluorescence quantum yield determined by a calibrated integrating sphere. ^d $\alpha_{\text{AIE}} = \Phi_{\text{F}}(\text{solid})/\Phi_{\text{F}}(\text{solution})$.

TPA-Py-2 were also lower than TPA-Py-7 series, (TPA-Py-2-Br: 63, TPA-Py-2-BF₄: 149, TPA-Py-7-Br: 234, TPA-Py-7-BF₄: 272).

Furthermore, by introducing the auxochrome of methoxy groups into the molecular structures, a stronger donor-acceptor effect resulted in shifting both absorption and emission peaks to the longer wavelength in DMSO solutions. The PL characteristics of diOMe-TPA-Py series are illustrated in Fig. S28–S31 (ESI[†]). The emission intensity of diOMe-TPA-2 series exhibited divergent ACQ behaviors (Fig. S28 and S29, ESI[†]) upon increasing the fraction of poor solvent. Nevertheless, the emission intensity of diOMe-TPA-7 series (Fig. S30 and S31, ESI[†]) was much enhanced as the fraction of water went up to 99%, and the PL intensity (I/I_0) of diOMe-TPA-7 series was about 2.7-fold for diOMe-TPA-Py-7-Br and 5.4-fold for diOMe-TPA-Py-7-BF₄, which was stronger than those in pure DMSO solutions, implying the AIE effect. Inferring from the results, diOMe-TPA-Py-2-Br and diOMe-TPA-Py-2-BF₄

exhibited AIE activity based on the α_{AIE} (>1), which was calculated by the PL quantum yields of those compounds in both solution state and solid state. However, while the AIE behaviors were investigated *via* water/DMSO system, the results of diOMe-TPA-Py-2-Br and diOMe-TPA-Py-2-BF₄ exhibited ACQ effect, which is contrary to the results based on the measurement of PL quantum yields. As a result, this phenomenon may be caused by the twisted intermolecular charge transfer (TICT), which plays a significant correlation with the AIE effect of the donor-acceptor (D–A) luminescent system. In general, the polar solvent, steric restrictions, and D–A efficacy and strength could have decisive impacts on the TICT phenomenon. Interpreting the structure of molecules, the methoxy group could enhance the electron-donating ability for triphenylamine, which would construct the more efficient D–A system with pyridinium salts to facilitate the TICT state, while the longer alkyl chain would

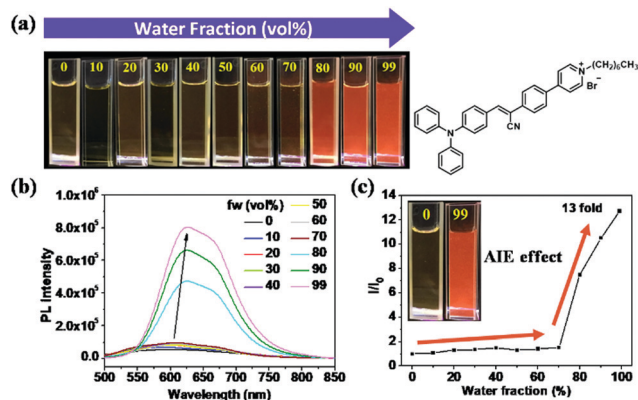


Fig. 3 (a) Photos taken under UV light of TPA-Py-7-Br in different water/DMSO fractions. (b) PL spectra of TPA-Py-7-Br in DMSO and water/DMSO solutions with different water fractions (f_w). (c) Plot of relative emission intensity (I/I_0) versus different compositions of aqueous mixtures of TPA-Py-7-Br. I_0 = emission intensity in pure DMSO solution (10 μ M). λ_{ex} : 451 nm.

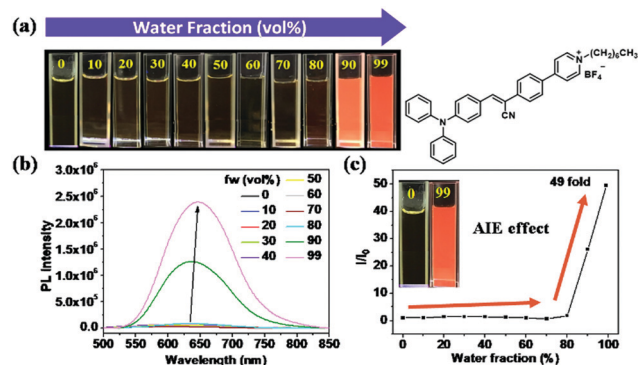


Fig. 4 (a) Photos taken under UV light of TPA-Py-7-BF₄ in different water/DMSO fractions. (b) PL spectra of TPA-Py-7-BF₄ in DMSO and water/DMSO solutions with different water fractions (f_w). (c) Plot of relative emission intensity (I/I_0) versus different compositions of aqueous mixtures of TPA-Py-7-BF₄. I_0 = emission intensity in pure DMSO solution (10 μ M). λ_{ex} : 451 nm.

easily hinder and restrict the TICT state. As a result, diOMe-TPA-Py-2-Br and diOMe-TPA-Py-2-BF₄ may show more obvious TICT effect than other molecules and result in the decrease of fluorescent intensity in the polar solvent system (water/DMSO). Furthermore, the PL wavelength would red-shift with the increase of the water fraction (Fig. S28b and S29b, ESI[†]). Consequently, diOMe-TPA-Py-2-Br and diOMe-TPA-Py-2-BF₄ exhibited ACQ properties in water/DMSO system because of TICT effect, which could be influenced by the polar solvent, D-A efficacy and steric restrictions.

Single-crystal data. Generally, the concept of aggregation-induced emission (AIE) is that non-emissive luminogens could be induced to emit *via* the aggregated formation. Therefore, the analysis of single crystals should be a representative and useful approach to explain the ideal aggregative formation of the examined molecules and their corresponding AIE behaviors. Herein, to further comprehend the relation between molecular

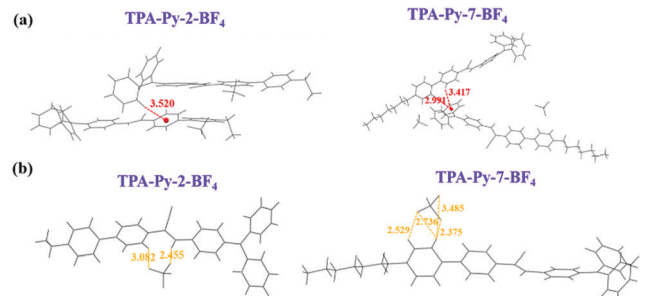


Fig. 5 Single-crystal data for the effect of the length of alkyl chain. (a) C-H... π interactions of TPA-Py-2-BF₄ and TPA-Py-7-BF₄. (b) C-H...F hydrogen bonds of TPA-Py-2-BF₄ and TPA-Py-7-BF₄.

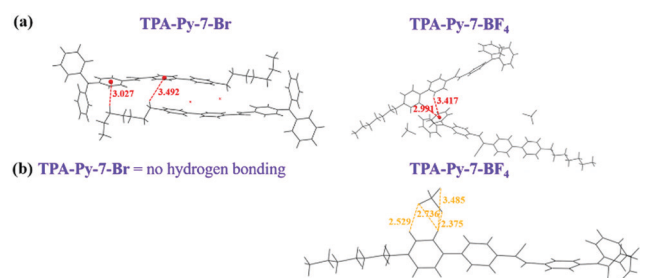


Fig. 6 Single-crystal data for the effect of different anions. (a) C-H... π hydrogen bonds of TPA-Py-7-Br and TPA-Py-7-BF₄. (b) C-H...F hydrogen bonds of TPA-Py-7-Br and TPA-Py-7-BF₄.

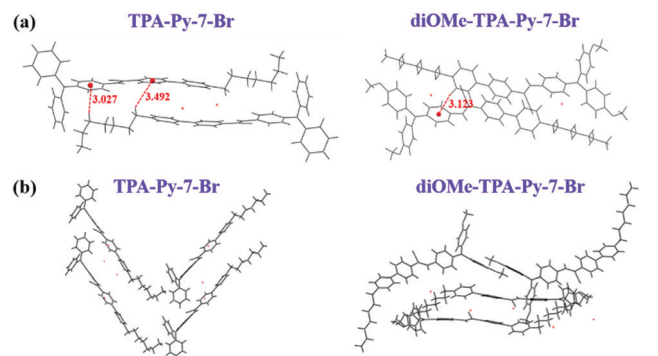


Fig. 7 Single-crystal data for the effect of dimethoxy substituents. (a) C-H... π hydrogen bonding of TPA-Py-7-Br and diOMe-TPA-Py-7-Br, which are denoted by dotted lines. (b) Perspective view of the packing arrangements in crystals of TPA-Py-7-Br and diOMe-TPA-Py-7-Br.

structures and photophysical properties of these luminogens in the solid state, their single crystals and packing models were obtained and investigated as shown in Fig. 5–7, and the detailed information is summarized in Tables S1–S5 (ESI[†]). According to these results, all intermolecular chains of these compounds exhibited C-H... π interaction with distances less than 3.5 Å between a face of an aromatic ring and another hydrogen atom within two molecular chains, resulting in AIE behavior in solid state. To investigate the phenomena as mentioned above and the effects of the alkyl chain length, TPA-Py-2-BF₄ was selected to compare with TPA-Py-7-BF₄ (Fig. 5). The latter exhibited shorter,

immobilized C-H... π interactions with distances of 2.991 Å and 3.417 Å, and more and shorter hydrogen bonds between hydrogens of the phenyl ring and the fluorine atoms of BF_4^- , with distances of 2.375 Å, 2.529 Å, 2.736 Å and 3.485 Å. That is, the motion between TPA-Py-7-BF_4 molecules can be restricted more effectively by C-H... π interactions, thus preventing the energy decay from non-radiative routes. Therefore, TPA-Py-7-BF_4 displayed higher solid-state quantum yield than TPA-Py-2-BF_4 , which is the same trend as previously reported.¹⁴ Furthermore, in order to disclose the anion effects of bromide and BF_4^- , the molecular models of conformation in single crystals of TPA-Py-7-Br and TPA-Py-7-BF_4 illustrated in Fig. 6 revealed that TPA-Py-7-BF_4 possessed not only C-H...F hydrogen bonds but also shorter C-H... π bonds. Consequently, TPA-Py-7-BF_4 exhibited stronger PL intensity in solid state than the corresponding molecular structure with bromide anion.¹⁵ Besides, TPA-Py-7-Br and diOMe-TPA-Py-7-Br were chosen as representatives to confirm the dimethoxy substituent effect; C-H... π bonds existed in both structures and without π - π stacking (Fig. 7a), while TPA-Py-7-Br displayed higher solid-state quantum yield than diOMe-TPA-Py-7-Br , which might be caused by the more regular packing in a unit cell, as depicted in Fig. 7b. Also, from the single-crystal data, the reason for the methoxy groups causing lower quantum yields both in solution state and solid state, while BF_4^- and heptane chain ($n = 7$) produce higher quantum yields in solid state, could be explained by the intermolecular interactions. Consequently, referring to the molecular structure, the α -cyanostilbene-containing redox-active triphenylamine (TPA) derivatives possessing both methoxy groups and shorter alkyl chain length ($n = 2$) simultaneously revealed lower quantum yields in this molecular system.

Electrochemical and electrochromic properties

Electrochemical redox behavior and HOMO/LUMO energy level. The electrochemical behaviors of these obtained materials with pyridinium salts were investigated *via* cyclic voltammetry (CV) using ITO glass as the working electrode in anhydrous *N,N*-dimethylformamide (DMF) with 0.1 M of TBAP as the supporting electrolyte under nitrogen atmosphere. The typical CV diagrams of oxidation–reduction process for the series of α -cyanostilbene-containing TPA derivatives are summarized in Fig. 8, and the oxidation potentials of TPA-Py-2-Br , TPA-Py-2-BF_4 , TPA-Py-7-Br , TPA-Py-7-BF_4 , diOMe-TPA-Py-2-Br , $\text{diOMe-TPA-Py-2-BF}_4$, diOMe-TPA-Py-7-Br and $\text{diOMe-TPA-Py-7-BF}_4$ are 1.35, 1.30, 1.40, 1.36, 1.04, 1.02, 1.06 and 1.05 V, respectively. Moreover, lower oxidative potentials could be produced by introducing electron-donating dimethoxy groups into the para-position of the TPA unit, indicating methoxy groups not only could effectively increase the electron density but also stabilize the charges in the whole molecular structure to enhance the electrochemical performance. Furthermore, the highest occupied molecular orbital (HOMO) and lowest unoccupied molecular orbital (LUMO) of these molecules could be calculated from the related redox potentials, and the results are listed in Table 2. From CV measurement (on the basis that ferrocene/ferrocenium is 4.8 eV below the vacuum level with $E_{\text{onset}} = 0.55 \text{ V}^{16}$), the HOMO and LUMO energy levels can be estimated from the potentials of oxidation and reduction

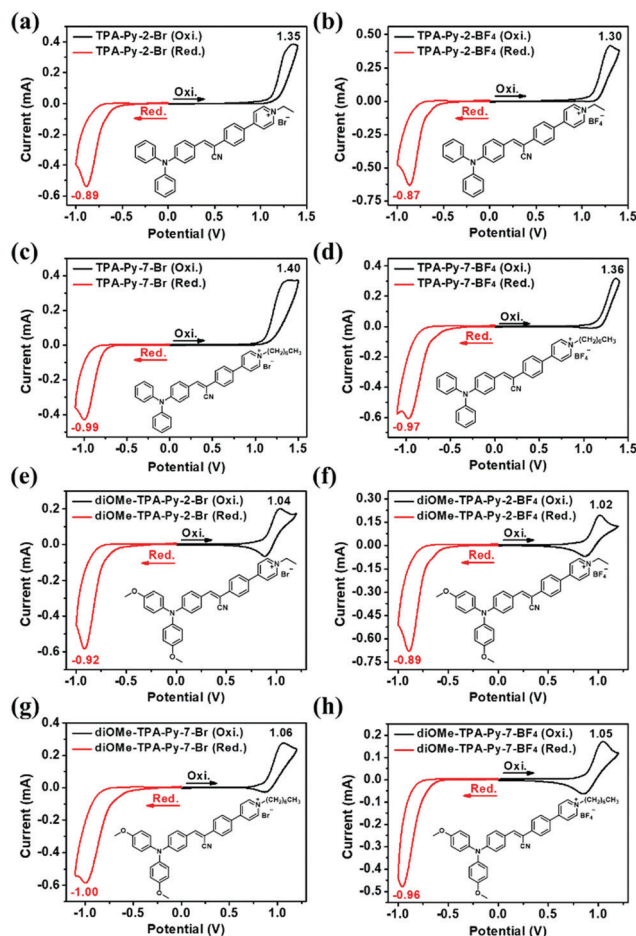


Fig. 8 Cyclic voltammetry diagrams (scan rate: 50 mV s^{-1}) of (a) TPA-Py-2-Br , (b) TPA-Py-2-BF_4 , (c) TPA-Py-7-Br , (d) TPA-Py-7-BF_4 , (e) diOMe-TPA-Py-2-Br , (f) $\text{diOMe-TPA-Py-2-BF}_4$, (g) diOMe-TPA-Py-7-Br and (h) $\text{diOMe-TPA-Py-7-BF}_4$ in DMF (10^{-3} M) containing 0.1 M of TBAP as the electrolyte and using an ITO glass as the working electrode.

Table 2 Redox potentials and energy levels of α -cyanostilbene-containing TPA derivatives

	Oxidation potential (vs. Ag/AgCl in DMF)		Reduction potential (V) (vs. Ag/AgCl in DMF)		
	$E_{\text{p,ox}}$ (V)	HOMO ^a (eV)	$E_{\text{p,red}}$ (V)	LUMO ^a (eV)	E_{g}^b (eV)
TPA-Py-2-Br	1.35	-5.60	-0.89	-3.36	2.24
TPA-Py-2-BF_4	1.30	-5.55	-0.87	-3.38	2.17
TPA-Py-7-Br	1.40	-5.65	-0.99	-3.26	2.39
TPA-Py-7-BF_4	1.36	-5.61	-0.97	-3.28	2.33
diOMe-TPA-Py-2-Br	1.04	-5.29	-0.92	-3.33	1.96
$\text{diOMe-TPA-Py-2-BF}_4$	1.02	-5.27	-0.89	-3.36	1.91
diOMe-TPA-Py-7-Br	1.06	-5.31	-1.00	-3.25	2.06
$\text{diOMe-TPA-Py-7-BF}_4$	1.05	-5.30	-0.96	-3.29	2.01

^a The HOMO and LUMO energy levels were calculated from CV and were referenced to ferrocene in TBAP/DMF (4.8 eV; onset = 0.55 V). ^b The data were calculated from the sample by the equation: $E_{\text{g}} = (E_{\text{p,ox}} - E_{\text{p,red}})$.

processes, respectively. Interestingly, while replacing bromide anion by BF_4^- , both the oxidative and reductive potentials exhibited lower values with the corresponding HOMO and LUMO

energy levels. On the other hand, if the longer alkyl chain length was incorporated into structures, higher oxidative and reductive potentials would be obtained.

Electrochemical stability. In order to explore the potential application of these resulting materials, the critical issue of electrochemical stability was verified by continuous CV scanning utilizing an optically transparent thin-layer electrochemical (OTTLE) cell in anhydrous propylene carbonate (PC) solution including 1 mM of analytes and 0.1 M of tetrabutylammonium tetrafluoroborate (TBABF₄) as the supporting electrolyte. The representative four redox-active target compounds with BF₄⁻ were chosen to conduct CV measurements under the electrolyte system with the same BF₄⁻ counter-anion. The typical differential pulse voltammetry (DPV) diagrams for these redox-active EC materials are illustrated in Fig. 9, and the oxidation potentials of TPA-Py-2-BF₄, TPA-Py-7-BF₄, diOMe-TPA-Py-2-BF₄ and diOMe-TPA-Py-7-BF₄ were 1.08, 1.12, 0.85 and 0.89 V, respectively. The DPV results for TPA-Py-2-BF₄ and TPA-Py-7-BF₄ after 50 and 100 scanning cycles, shown in Fig. 9a and b, respectively, revealed slightly different values of E_{onset} compared to the first cycle due to the formation of benzidine structure by coupling dimerization. Nevertheless, DPV diagrams of diOMe-TPA-Py-2-BF₄ and diOMe-TPA-Py-7-BF₄ with the dimethoxy groups depicted in Fig. 9c and d exhibited not only lower oxidation potentials and higher electrochemical stability than TPA-Py-2-BF₄ and TPA-Py-7-BF₄, but also no additional peak in their DPV diagrams, confirming that no dimer structure could be generated during the redox reaction.^{6c,d} From the perspective of alkyl chain length effect, it showed similar electrochemical behaviors regardless of which alkyl chain length was incorporated.

Electrochromic characteristics by spectroelectrochemical measurements. The spectroelectrochemical measurements were also conducted to demonstrate the EC behaviors of the resulting materials by OTTLE coupled with UV-vis spectroscopy. The typical optical absorption spectra and the related EC coloring behaviors of TPA-Py-2-BF₄, TPA-Py-7-BF₄, diOMe-TPA-Py-2-BF₄ and diOMe-TPA-Py-7-BF₄ are shown in Fig. 10. The absorption

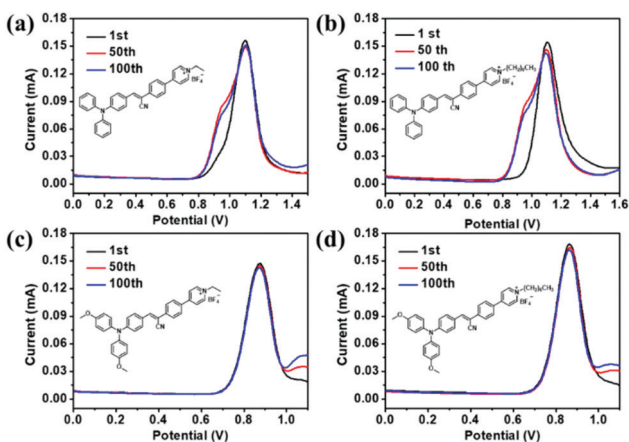


Fig. 9 Differential pulse voltammogram (scan rate: 5 mV s⁻¹; pulse amplitude: 50 mV; pulse width: 50 ms; pulse period: 0.2 s) at a concentration of 10⁻³ M for (a) TPA-Py-2-BF₄, (b) TPA-Py-7-BF₄, (c) diOMe-TPA-Py-2-BF₄, (d) diOMe-TPA-Py-7-BF₄ for the 1st, 50th, and 100th cycles in 0.1 M TBABF₄/PC solution.

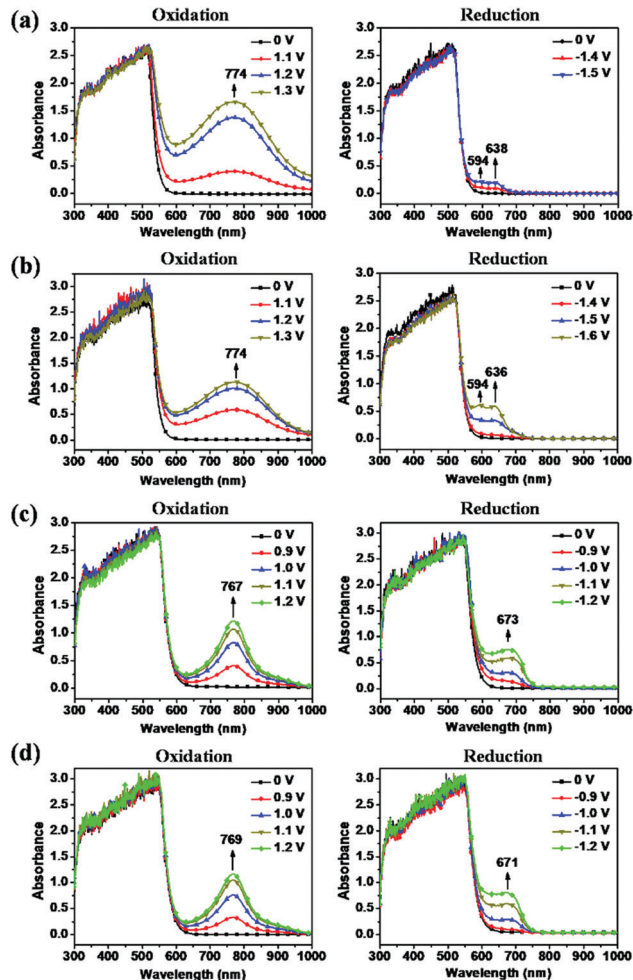


Fig. 10 Spectroelectrochemical absorption spectra of (a) TPA-Py-2-BF₄, (b) TPA-Py-7-BF₄, (c) diOMe-TPA-Py-2-BF₄, and (d) diOMe-TPA-Py-7-BF₄ at different applied potentials during oxidation and reduction. Concentration of the materials was 10⁻³ M dissolved in 0.1 M of TBABF₄/PC.

spectrum of TPA-Py-2-BF₄ displayed high absorbance between 300–550 nm at the neutral form, with the color of pale orange. Upon oxidation, a new absorption peak (774 nm) would arise with increasing intensity, attributed to the formation of radical-cation structure caused by mono-electron oxidation of the TPA unit. In addition, two new peaks appeared at 594 and 638 nm during reduction. The UV-vis absorption spectra of TPA-Py-7-BF₄ depicted in Fig. 10b revealed a strong absorption band in the range of 300–500 nm for the neutral form, and an obvious peak at 774 nm came out once oxidation occurred from 0 V to 1.3 V. For diOMe-TPA-Py-2-BF₄, the new characteristic peak at 767 nm emerged upon oxidation by applying voltage from 0 V to 1.2 V, and a new absorption band at 673 nm showed up, with applied potential from 0 V to -1.2 V for reduction, as depicted in Fig. 10c. Similarly, Fig. 10d exhibited the optical absorption change of diOMe-TPA-Py-7-BF₄ from 0 V to 1.2 V and 0 V to -1.2 V for oxidation and reduction processes, revealing a similar neutral absorption peak and new absorption characteristic peaks at 769 nm and 671 nm for oxidation and reduction, respectively.

Conclusions

A series of AIE-active α -cyanostilbene-containing TPA derivatives with pyridinium salts, **TPA-Py-*n*-Br**, **TPA-Py-*n*-BF₄**, **diOMe-TPA-Py-*n*-Br** and **diOMe-TPA-Py-*n*-BF₄**, were successfully synthesized. Different alkyl chain lengths and anions were incorporated through simple alkylation reaction and ion exchange process, and the molecular structure effects on electrochemical behaviors, optical characteristics, and PL properties were investigated and discussed in this study. From the results, the optical absorption characteristics for both solution and solid states changed very slightly despite replacing Br⁻ with BF₄⁻ but exhibited a bathochromic effect as a longer alkyl chain length was incorporated. As to the PL emission in solution state, the molecular structures with longer alkyl chain length and BF₄⁻ anion resulted in a red-shift effect. However, the molecules with longer alkyl chain length would induce the hypsochromic emission shift in solid state due to the weaker interaction between the aromatic molecules in the lattice. From the perspective of PL quantum yield, the longer alkyl chain and replacement of Br⁻ by BF₄⁻ anion would generate higher quantum yield, because the longer alkyl chain not only could significantly alter the intermolecular arrangement and interaction but cause a larger steric effect to prevent close π - π stacking. In addition, compared to the intermediate compounds of **TPA-CNBr** and **diOMe-TPA-CNBr**, the new corresponding materials of **TPA-Py-*n*-Br** and **diOMe-TPA-Py-*n*-BF₄** obtained in this work revealed ambipolar electrochemical and EC behaviors as pyridinium salt moieties were incorporated into the molecular structures.

Conflicts of interest

There are no conflicts to declare.

Acknowledgements

This work was financially supported by the “Advanced Research Center for Green Materials Science and Technology” from The Featured Area Research Center Program within the framework of the Higher Education Sprout Project by the Ministry of Education (108L9006) and the Ministry of Science and Technology in Taiwan (MOST 108-3017-F-002-002, 107-2113-M-002-024-MY3, and 107-2221-E-002-066-MY3).

Notes and references

- (a) Z. M. Zhang and D. B. McCormick, *Proc. Natl. Acad. Sci. U. S. A.*, 1991, **88**, 10407; (b) I. Mancini, A. Sicurelli, G. Guella, T. Turk, P. Maček and K. Sepčí, *Org. Biomol. Chem.*, 2004, **2**, 1368.
- (a) S. Aryal, C.-M. J. Hu and L. Zhang, *Small*, 2010, **6**, 1442; (b) M. Markiewicz, M. Piszora, N. Caicedo, C. Jungnickel and S. Stolte, *Water Res.*, 2013, **47**, 2921; (c) N. Mas, A. Agostini, L. Mondragón, A. Bernardos, F. Sancenón, M. D. Marcos, R. Martínez-Máñez, A. M. Costero, S. Gil, M. Merino-Sanjuán, P. Amorós, M. Orzáez and E. Pérez-Payá, *Chem. – Eur. J.*, 2013, **19**, 1346; (d) Y. Huang, G. Zhang, F. Hu, Y. Jin, R. Zhao and D. Zhang, *Chem. Sci.*, 2016, **7**, 7013.
- G. Niu, R. Zhang, Y. Gu, J. Wang, C. Ma, R. T. K. Kwok, J. W. Y. Lam, H. H.-Y. Sung, I. D. Williams, K. S. Wong, X. Yu and B. Z. Tang, *Biomaterials*, 2019, **208**, 72.
- (a) N. Zhao, M. Li, Y. Yan, J. W. Y. Lam, Y. L. Zhang, Y. S. Zhao, K. S. Wong and B. Z. Tang, *J. Mater. Chem. C*, 2013, **1**, 4640; (b) K. Tanabe, Y. Suzui, M. Hasegawa and T. Kato, *J. Am. Chem. Soc.*, 2012, **134**, 5652.
- J. Luo, Z. Xie, J. W. Y. Lam, L. Cheng, H. Chen, C. Qiu, H. S. Kwok, X. Zhan, Y. Liu, D. Zhu and B. Z. Tang, *Chem. Commun.*, 2001, 1740.
- (a) W. Z. Yuan, P. Lu, S. Chen, J. W. Y. Lam, Z. Wang, Y. Liu, H. S. Kwok, Y. Ma and B. Z. Tang, *Adv. Mater.*, 2010, **22**, 2159; (b) Y. Hong, J. W. Y. Lam and B. Z. Tang, *Chem. Soc. Rev.*, 2011, **40**, 5361; (c) Q. Zhao, S. Zhang, Y. Liu, J. Mei, S. Chen, P. Lu, A. Qin, Y. Ma, J. Z. Sun and B. Z. Tang, *J. Mater. Chem.*, 2012, **22**, 7387; (d) X. Y. Shen, Y. J. Wang, H. Zhang, A. Qin, J. Z. Sun and B. Z. Tang, *Chem. Commun.*, 2014, **50**, 8747.
- (a) D. C. Huang, J. T. Wu, Y. Z. Fan and G. S. Liou, *J. Mater. Chem. C*, 2017, **5**, 9370; (b) J. T. Wu and G. S. Liou, *Chem. Commun.*, 2018, **54**, 2619; (c) H. J. Yen and G. S. Liou, *Polym. Chem.*, 2018, **9**, 3001; (d) H. J. Yen and G. S. Liou, *Prog. Polym. Sci.*, 2019, **89**, 250.
- C. Y. Y. Yu, H. Xu, S. Ji, R. T. K. Kwok, J. W. Y. Lam, X. Li, S. Krishnan, D. Ding and B. Z. Tang, *Adv. Mater.*, 2017, **29**, 1606167.
- (a) S. Zeng, L. Yin, X. Jiang, Y. Li and K. Li, *Dyes Pigm.*, 2012, **95**, 229; (b) A. X. Ding, H. J. Hao, Y. G. Gao, Y. D. Shi, Q. Tang and Z. L. Lu, *J. Mater. Chem. C*, 2016, **4**, 5379; (c) S. Y. Chen, Y. W. Chiu and G. S. Liou, *Nanoscale*, 2019, **11**, 8597.
- (a) S. Zeng, L. Yin, C. Ji, X. Jiang, K. Li, Y. Li and Y. Wang, *Chem. Commun.*, 2012, **48**, 10627; (b) A. X. Ding, H. J. Hao, Y. G. Gao, Y. D. Shi, Q. Tang and Z. L. Lu, *J. Mater. Chem. C*, 2016, **4**, 5379.
- A. Pană, A. L. Panait and V. Cîrcu, *Res. Chem. Intermed.*, 2018, **44**, 2025.
- (a) R. Holomb, A. Martinelli, I. Albinsson, J. C. Lassègues, P. Johansson and P. Jacobsson, *J. Raman Spectrosc.*, 2008, **39**, 793; (b) A. J. Blake, S. J. Hill, P. Hubberstey and W. S. Li, *J. Chem. Soc., Dalton Trans.*, 1997, 913; (c) R. L. Hunt and B. S. Ault, *Spectrochim. Acta, Part A*, 1981, **37**, 63.
- J. Dong, K. M. Solntsev and L. M. Tolbert, *J. Am. Chem. Soc.*, 2009, **131**, 662.
- (a) A. S. Blum, M. H. Moore and B. R. Ratna, *Langmuir*, 2008, **24**, 9194; (b) X. Shen, G. Huang, K. Li, G. Zhang and D. Zhang, *Sci. China: Chem.*, 2013, **56**, 1197; (c) A. S. Blum, M. H. Moore and B. R. Ratna, *Langmuir*, 2008, **24**, 9194.
- J. Wang, X. Gu, P. Zhang, X. Huang, X. Zheng, M. Chen, H. Feng, R. T. K. Kwok, J. W. Y. Lam and B. Z. Tang, *J. Am. Chem. Soc.*, 2017, **139**, 16974–16979.
- S. Miao, H. Li, Q. Xu, N. Li, J. Zheng, R. Sun, J. Lu and C. M. Li, *J. Mater. Chem.*, 2012, **22**, 16582.